ELEMENTA
Science of the Anthropocene

Heuzé, C and Årthun, M. 2019. The Atlantic inflow across the Greenland-Scotland ridge in global climate models (CMIP5). *Elem Sci Anth,* 7: 16. DOI: https://doi.org/10.1525/elementa.354

RESEARCH ARTICLE

The Atlantic inflow across the Greenland-Scotland ridge in global climate models (CMIP5)

Céline Heuzé* and Marius Årthun†,‡

Oceanic heat transport from the North Atlantic to the Arctic through the Nordic Seas is a key component of the climate system that has to be modelled accurately in order to predict, for example, future Arctic sea ice changes or European climate. Here we quantify biases in the climatological state and dynamics of the transport of oceanic heat into the Nordic Seas across the Greenland-Scotland ridge in 23 state-of-the-art global climate models that participated in the Climate Model Intercomparison Project phase 5. The mean poleward heat transport, its seasonal cycle and interannual variability are inconsistently represented across these models, with a vast majority underestimating them and a few models greatly overestimating them. The main predictor for these biases is the resolution of the model via its representation of the Greenland-Scotland ridge bathymetry: the higher the resolution, the larger the heat transport through the section. The second predictor is the large-scale ocean circulation, which is also connected to the bathymetry: models with the largest heat transport import water from the European slope current into all three straits of the Greenland-Scotland ridge, whereas those with a weak transport import water from the Labrador Sea. The third predictor is the spatial pattern of their main atmospheric modes of variability (North Atlantic Oscillation, East Atlantic and Scandinavian patterns), where the models with a weak inflow have their atmospheric low-pressure centre shifted south towards the central Atlantic. We argue that the key to a better representation of the large-scale oceanic heat transport from the North Atlantic to the Arctic in global models resides not only in higher resolution, but also in a better bathymetry and representation of the complex ocean-ice-atmosphere interactions.

Keywords: Oceanic heat transport; Nordic Seas; CMIP5 models; Climate models

Introduction

The Nordic Seas are the main gateway between the North Atlantic and the Arctic Ocean, and where the warmth of the northernmost extension of the Gulf Stream meets the cold Arctic (**Figure 1**). The associated poleward transport of oceanic heat into and through the Nordic Seas over the Greenland-Scotland ridge (GSR) has been found to influence, and accordingly provide a predictive potential for, Arctic sea ice (Årthun et al., 2012; Onarheim et al., 2015; Yeager et al., 2015) and the adjacent continental climate (Collins et al., 2006; Matei et al., 2012; Årthun et al., 2017). A realistic representation of the poleward ocean heat transport through the Nordic Seas in numerical models therefore seems to be a prerequisite to achieve skillful near-term climate predictions (Langehaug et al., 2017; Yeager and Robson, 2017) and long-term projections for the Arctic region (Mahlstein and Knutti, 2011; Burgard and Notz, 2017). The Atlantic inflow also influences the overflow of dense water across the GSR into the North Atlantic (Eldevik et al., 2009; Sandø et al., 2012) which is the main source of North Atlantic deep water (Dickson and Brown, 1994), and, hence, a key component of the Atlantic meridional overturning circulation (AMOC).

The poleward ocean heat transport through the Nordic Seas is carried by the two-branch Norwegian Atlantic Current (NwAC), extending from the gaps between Iceland and Scotland through to the Barents Sea and the Fram Strait (Orvik and Niiler, 2002; Østerhus et al., 2005; Skagseth et al., 2008). The exchange across the GSR takes place in three narrow passages: the Denmark Strait (DS), across the Iceland-Faroe Ridge (IFR), and through the Faroe-Shetland/Scotland Channel (FSC; **Figure 1**). The source waters of the NwAC predominantly come from the North Atlantic Current, the northern extension of the Gulf Stream, and from the European slope current that originates in the eastern subtropical Atlantic (Hansen and Østerhus, 2000). The relative contributions of these two sources influence the hydrographic properties of the Atlantic inflow across the GSR, and are related to large-scale ocean circulation in the North Atlantic (Hátún et al., 2005). Variations in the strength of the flow across the GSR have also been associated with changes in the local wind stress,

* Department of Earth Sciences, University of Gothenburg, SE
† Geophysical Institute, University of Bergen, Bergen, NO
‡ Bjerknes Centre for Climate Research, Bergen, NO
Corresponding author: Céline Heuzé (celine.heuze@gu.se)

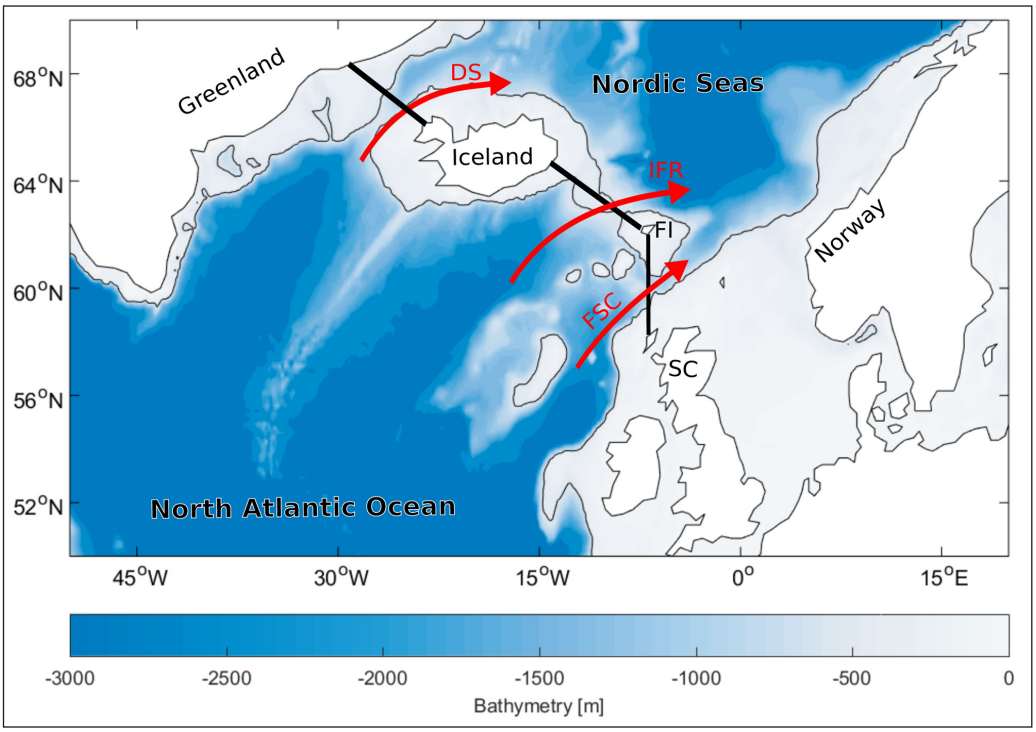

Figure 1: The main basins and connecting gateways between the North Atlantic and Nordic Seas. The major pathways of poleward ocean heat transport are indicated by the red arrows, the sections used to calculate transports are shown by the black lines, and bathymetry is indicated by the colour scale; DS: Denmark Strait; IFR; Iceland–Faroe Ridge; FSC: Faroe–Shetland/Scotland Channel. Also indicated are the Faroe Islands (FI) and Scotland (SC). DOI: https://doi.org/10.1525/elementa.354.f1

represented by the North Atlantic Oscillation (Biastoch et al., 2003; Richter et al., 2012; Sandø et al., 2012), although the details of the mechanism are debated and depend on the inflow branch considered (Hansen et al., 2010).

The poleward transport of heat and salt varies widely among fully coupled climate models (Deshayes et al., 2014; Sandø et al., 2014; Li et al., 2017; Menary and Wood, 2017), and the complex geometry of the GSR makes it a challenging task for coarse-resolution climate models to realistically represent the water mass exchanges between the subpolar North Atlantic and the Nordic Seas (Danabasoglu et al., 2010; Guo et al., 2016; Olsen et al., 2016). Yet models are the best tools to date to assess climate variability and change; hence, ascertaining to what extent models skillfully simulate the heat exchanges across the GSR and into the Arctic is of critical importance.

Here, we present the first multi-model assessment of the poleward ocean heat transport through all three gateways to the Nordic Seas, using 23 state-of-the-art global climate models that participated in the Climate Model Intercomparison Project phase 5 (CMIP5; Taylor et al., 2012). In this study we first evaluate the simulated heat transport with respect to the observed flow across the GSR, which has been monitored since the mid 1990s (Østerhus et al., 2005). We then identify causes for these biases in the design and dynamics of the CMIP5 models before discussing some possible ways to improve the models. We finish with some concluding remarks notably on the need for continuous observational time series in such critical regions.

Data and Methods

CMIP5 models

We used the monthly output of ocean temperature, salinity and velocities, and sea level pressure from the historical run over the period 1986–2005 of 23 fully coupled CMIP5 models (**Table 1**). These models were chosen in order to have a wide diversity in the ocean model component, in modelling centres, in resolution, and in vertical grid type. We used only one ensemble member for each model (r1i1p1) as it is the only one available for all the models.

As most models have a tripolar horizontal grid, following Menary et al. (2015) we provide in **Table 1** their effective horizontal resolution; that is, the average distance between two points in the Nordic Seas. The effective horizontal model resolution varies from 0.2° (MPI-ESM-LR) to 3° (CMCC-CMS) in latitude. As most models have different vertical grid spacings as well, by analogy we also provide in **Table 1** the effective vertical resolution; that is, the number of vertical levels in the Greenland-Scotland Ridge, between the surface and 500 m. This effective vertical resolution ranges from 33 levels in CCSM4 and CESM1 (CAM5) to only 9 levels for GISS-E2-R. The majority of models have z or z*-level vertical grids, where z indicates a standard fixed-depth vertical grid and z*, one with a free surface. Four of them were run on an isopycnal (GFDL-ESM2G) or hybrid (MIROC5 and -ESM-CHEM, NorESM1-M) grid, but their output was provided on a regular z-level grid.

Table 1: Details of the CMIP5 models (after Flato et al., 2013) used in this study. DOI: https://doi.org/10.1525/elementa.354.t1

	Model name	Ocean component	Eff. horiz. res.[a] (° latitude)	Eff. vertical res.[b]	Vertical grid[c]
1.	MPI-ESM-LR	MPIOM	0.2	18	z
2.	CCSM4	POP2	0.4	33	z
3.	CESM1 (CAM5)	POP2	0.4	33	z
4.	NorESM1-M	own	0.4	27	z-ρ
5.	MPI-ESM-MR	MPIOM	0.4	18	z
6.	MIROC5	COCO4.5	0.4	23	z-σ
7.	ACCESS1.0	MOM4p1	0.5	26	z*
8.	CNRM-CM5	NEMO	0.8	22	z
9.	GFDL-ESM2G	GOLD	0.8	30	ρ
10.	HadGEM2-CC	own	0.9	22	z
11.	HadGEM2-ES	own	0.9	22	z
12.	FGOALS-g2	LICOM2	0.9	20	z*
13.	BCC-CSM1.1	MOM4L40	1.0	26	z
14.	GFDL-CM3	MOM4.1	1.0	30	z*
15.	GFDL-ESM2M	MOM4.1	1.0	30	z*
16.	GISS-E2-R	Russell	1.2	9	z*
17.	CanESM2	own	1.3	22	z
18.	CSIRO-Mk3.6.0	MOM2.2	1.6	15	z
19.	MIROC-ESM-CHEM	COCO3.4	1.9	21	z-σ
20.	CMCC-CM	OPA8.2	3.0	19	z
21.	CMCC-CMS	OPA8.2	3.0	19	z
22.	IPSL-CM5A-LR	own	3.0	19	z
23.	IPSL-CM5A-MR	own	3.0	19	z

[a] Effective horizontal resolution is the average distance between two grid points in the Nordic seas for each model (see Methods).
[b] Effective vertical resolution is the number of levels above 500 m (see Methods).
[c] Letter z indicates a standard fixed-depth vertical grid; z*, one with a free surface; ρ, an isopycnic grid; σ, a terrain-following grid; and two symbols, a hybrid grid.

Methodology: heat transport

Monthly oceanic "heat transport" Q through the Denmark Strait, the Iceland-Faroe Ridge, and the Faroe-Scotland Channel was computed from the monthly potential temperature θ and velocities after interpolation onto the sections defined on **Figure 1**, as:

$$Q = \int_A c_p \rho_\theta (\theta - \theta_{ref}) \mathbf{V} dA, \quad (1)$$

where A is the section area, c_p = *3980* J kg^{-1} K^{-1} is the specific heat capacity of water, ρ_θ is the potential density (Fofonoff and Millard Jr, 1983), and **V** is the velocity perpendicular to the section considered. Note that Equation 1 does not provide the actual oceanic heat transport through the section, as that would require a closed volume budget across the GSR (Schauer and Beszczynska–Möller, 2009). Here we instead computed the heat flux through the section relative to a reference temperature θ_{ref} = 0°C, chosen to enable comparison with the presented observational estimates and that is based on the observation that the southward flow across the GSR is close to this temperature (Hansen et al., 2003). However, to facilitate the reading and interpretation of this manuscript, the heat flux through the GSR relative to θ_{ref} that we computed is referred to as the heat transport.

We used the most up-to-date observational estimates of heat transport across the GSR to evaluate the CMIP5 models. For the DS, Jónsson and Valdimarsson (2012) found a mean poleward heat transport between 1994 and 2010 of 24 ± 4 TW (the error estimate was reported as <15%); for the IFR, Hansen et al. (2015) reported 124 ± 15 TW for 1993–2013, and for the FSC between 1994 and 2011, Berx et al. (2013) calculated 107 ± 21 TW. Unfortunately, these estimates are based on measurements since the mid

1990s, and, hence, do not overlap completely with the time period considered for the models. Although we do not consider this incomplete overlap to be a major source of discrepancy between the observations and the models, as the observed interannual variabilities are low compared to the mean values, we also briefly compare the CMIP5 models to the 1986–2005 average of one state estimate, GECCO2 (German contribution of the Estimating the Circulation and Climate of the Ocean project; Köhl 2015), and two reanalysis products, OraS4 (Ocean ReAnalysis System 4; Balmaseda et al., 2013) and SODA3.3.1 (Simple Ocean Data Assimilation; Carton and Giese, 2008). Admittedly, the ocean state estimate and reanalyses are also based on models, but as they are constrained to ocean observations and forced by a realistic atmospheric circulation, we nevertheless expect them to adequately represent the mean Atlantic heat transport toward the Arctic (Uotila et al., 2018).

Methodology: backtracking

Suspecting that the coarse resolution models may struggle to correctly represent the bathymetry-controlled import of water towards the GSR, we determined the North Atlantic sources of the water crossing the GSR. As models do not provide any sort of passive tracer, we had to perform our own simple backtracking.

The first step for the backtracking was to compute for each model the month-to-month deformation of its original grid using the monthly mean horizontal ("uo" and "vo") and vertical velocities ("wo"). Considering a grid cell at a given longitude, latitude and depth at the first time step, we computed its longitudinal displacement caused by advection over one month with a zonal velocity uo, latitudinal displacement caused by the meridional velocity vo, and vertical displacement caused by wo. If either of these displacements was larger than the cell's dimension, we considered that the water had moved to a different grid cell. This new grid cell position is what we recorded in the deformation matrix. We then computed the longitudinal, latitudinal and vertical displacements after one month of this new grid cell, and so on until the end of our twenty-year period. Starting at the centre of the grid instead of a corner and/or recording displacements within the same grid cell yields no significant difference in trajectories (not shown). Unfortunately, the vertical velocity wo is not a standard CMIP5 output and had to be computed from the vertical mass displacement ("wmo") divided for each grid cell by the water density in that cell and the cell area. Two models, GFDL-ESM2G and MIROC-ESM-CHEM, do not provide wmo and hence were not included in the backtracking analysis.

Our second and final step consisted of identifying from the deformation matrix, for each time step, which "deformed" cells are in either strait of the Greenland-Scotland Ridge. Using the deformation matrix, we went back in time and obtained all the previous positions of that cell up until the beginning of the study period. No distinction was made between poleward and southward trajectories in these calculations, as individual snapshots (not shown) revealed that many models seem to have complex recirculations. What we have obtained here is a very simple trajectory model. We only have monthly mean velocities, and neither eddy fluxes nor diffusion can be taken into account despite their influence on the Lagrangian pathways (Drijfhout et al., 2003; Brambilla and Talley, 2006). Our results are used only to get a coarse estimate of the source regions.

Methodology: potential drivers

To investigate the potential causes for any encountered heat transport misrepresentation, we computed for each section the heat and volume transports and the temperature across the sections. We concentrated on the poleward heat and volume transports, i.e. crossing the GSR from the North Atlantic into the Nordic Seas. We define the 20-year mean heat transport value as the mean of the twenty yearly means; the interannual variability as the standard deviation of the twenty yearly means; and the seasonal variability as the mean of the maximum-to-minimum amplitudes obtained for each calendar year.

In addition, we assessed whether the model differences can be related to different dominant drivers of oceanic variability in the North Atlantic region:

1) The AMOC at 45°N was calculated by integrating the (resolved) meridional velocity from coast to coast, and then over depth using the bottom of the ocean as the reference level. The AMOC strength was then defined as the maximum southward transport (e.g. Heuzé 2017).
2) The subpolar gyre (SPG) strength, which is the leading mode of sea surface height (SSH) variability in the subpolar North Atlantic (Häkkinen and Rhines, 2004; Hátún and Chafik, 2018), was calculated as the first empirical orthogonal function (EOF) between 70°W and 20°E. The SPG strength inferred from SSH showed similar temporal variability to that based on the barotropic streamfunction, although their associated spatial pattern of variability could differ (Langehaug et al., 2012).

The dominant modes of atmospheric circulation variability were calculated by an EOF analysis of sea level pressure. For all models the three leading modes are:

1) EOF1: the North Atlantic Oscillation (NAO; Hurrell 1995), characterised by a low pressure system centered over Iceland and a high pressure anomaly over the Azores;
2) EOF2: the East Atlantic Pattern (EA; Barnston and Livezey, 1987), characterised by a low pressure system around the Bay of Biscay;
3) and EOF3: the Scandinavian Pattern (SCA; also referred to as Eurasian Type 1; Barnston and Livezey, 1987), characterised by a low pressure system over Scandinavia and a weaker high-pressure anomaly over Greenland.

As was highlighted by Davini and Cagnazzo (2014), for some models the order of the EOFs does not match that of the real world, and the EOF1, for example, actually represents the EA instead of the NAO. Hence in this manu-

script, for each model, we have defined the indices based on the location of their low pressure system rather than on the order of their EOF.

For both the oceanic and atmospheric drivers, the associated indices used in the statistical analysis were defined using the corresponding principal component time series. When calculating instantaneous correlations between heat transports and the defined indices of large-scale oceanic and atmospheric variability, the long term mean seasonal cycle was removed from all the monthly time series by subtracting the 20-year mean of each month. In addition, a 12-month running mean was sometimes applied to the time series to highlight interannual variability.

Modelled mean state of poleward heat transport

Climatological biases

We first quantified biases in poleward heat transport into the Nordic Seas in the individual models, and investigated whether these can consistently be explained with across-model relationships between the biases and the properties of the models.

The majority of CMIP5 models have weaker poleward heat transports than the observations and reanalyses in Denmark Strait and the Iceland Faroe Ridge, except for a few that greatly exceed the observational values (black line, **Figure 2**). In contrast, in the Faroe-Scotland Channel, the majority of models have stronger transport than reported in observations by Berx et al. (2013). There is no compensation in place for CMIP5 models. That is, a too-strong transport in one strait is not consistently associated with a weak transport in another. For example, HadGEM2-CC and HadGEM2-ES have strong transports in all three straits, whereas MIROC-ESM-CHEM is too weak in DS (20-year mean of 6 TW, **Figure 2a**), the strongest in IFR (318 TW, **Figure 2b**), but quite accurate in FSC (159 TW, **Figure 2c**). The multimodel mean of total poleward heat transport across the GSR is 274 TW, which is stronger than the observed 254 TW. The spread is very large, however, with total poleward heat transports ranging from 61 TW in IPSL-CM5A-LR to 630 TW in FGOALS-g2.

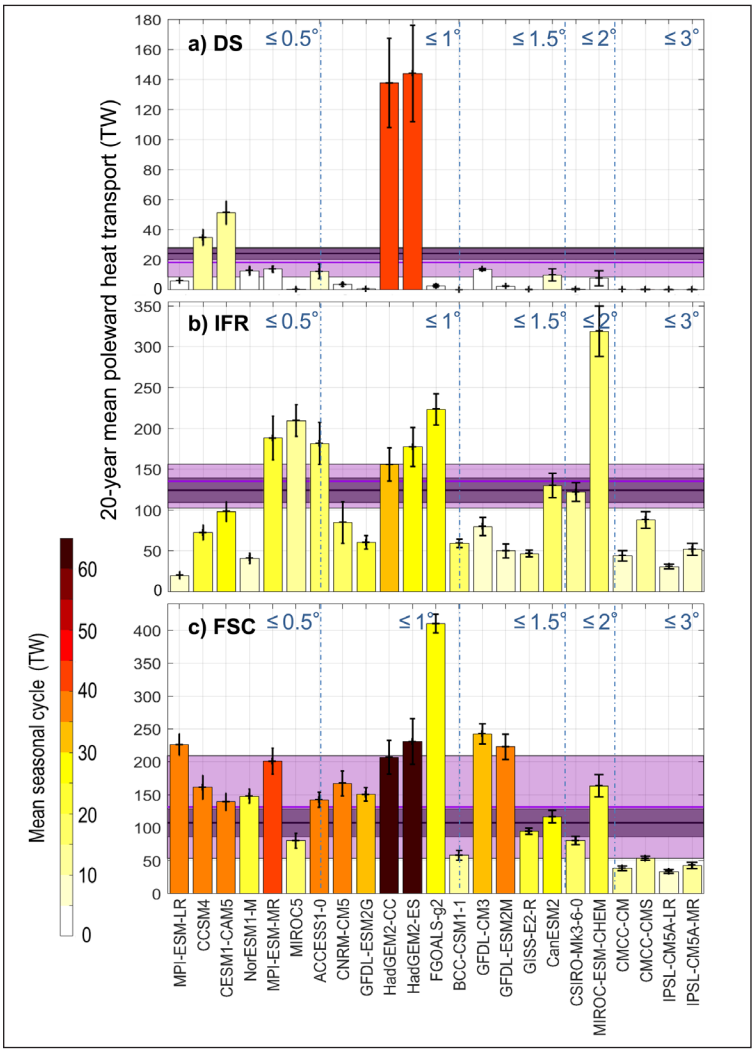

Figure 2: Mean biases in poleward heat transport through the three gateways. For the 23 CMIP5 models ordered by effective horizontal resolution (quoted in blue) as in Table 1, 20-year mean poleward heat transport in TW (bar), interannual variability in TW (black error bar), and mean seasonal cycle in TW (shading) for **a)** Denmark Strait (DS); **b)** the Iceland-Faroe Ridge (IFR); **c)** the Faroe-Scotland Channel (FSC). Note the different y-axes. For each panel, black horizontal line is the mean observed value and grey shading its uncertainty; purple line with lilac shading, the mean and uncertainty of the reanalyses (see Data and Methods). DOI: https://doi.org/10.1525/elementa.354.f2

The CMIP5 models also exhibit a very large spread in their representation of interannual (vertical bars, **Figure 2**) and seasonal (shading) heat transport variability. This spread is true whether we consider the absolute value or the percentage of the 20-year mean. The simulated variability is weaker than observed in DS and IFR, except for a few models that greatly overestimate it (e.g. HadGEM2-CC in DS, 30 TW compared to 4 in observations; **Figure 2a**). In FSC, all models underestimate the interannual variability (approx. 20 TW) with the exception of HadGEM-CC and -ES. We find similar results for the seasonal cycle: that of HadGEM-CC and -ES largely exceed the 10 TW observed in DS (Jónsson and Valdimarsson, 2012), 13 TW in IFR (Hansen et al., 2015) or 16 TW in FSC (Østerhus et al., 2005). There is in fact a strong positive correlation between the mean value and the strength of both the interannual and seasonal variabilities in the CMIP5 models.

The CMIP5 models disagree on the shape of the seasonal cycle (**Figure 3**). In DS, where the observed maximum is in August (Jónsson and Valdimarsson, 2012), six models have their maximum in winter. In IFR, the spread among the CMIP5 models is even larger, with only eight models having their maximum in October–November as in observations (Hansen et al., 2015). Lastly, in FSC, although all the models agree that the minimum of the seasonal cycle is in summer (blue colours on **Figure 3c**), there are maxima in all months between September and April.

We have demonstrated that there is a large spread across the CMIP5 models in the mean heat transported from the North Atlantic to the Nordic Seas, across the GSR, in the magnitude of the variability, and in the phase of the seasonal cycle. In the rest of this paper, we will show that these differences are mainly controlled by three interconnected factors: the horizontal resolution, the modelled

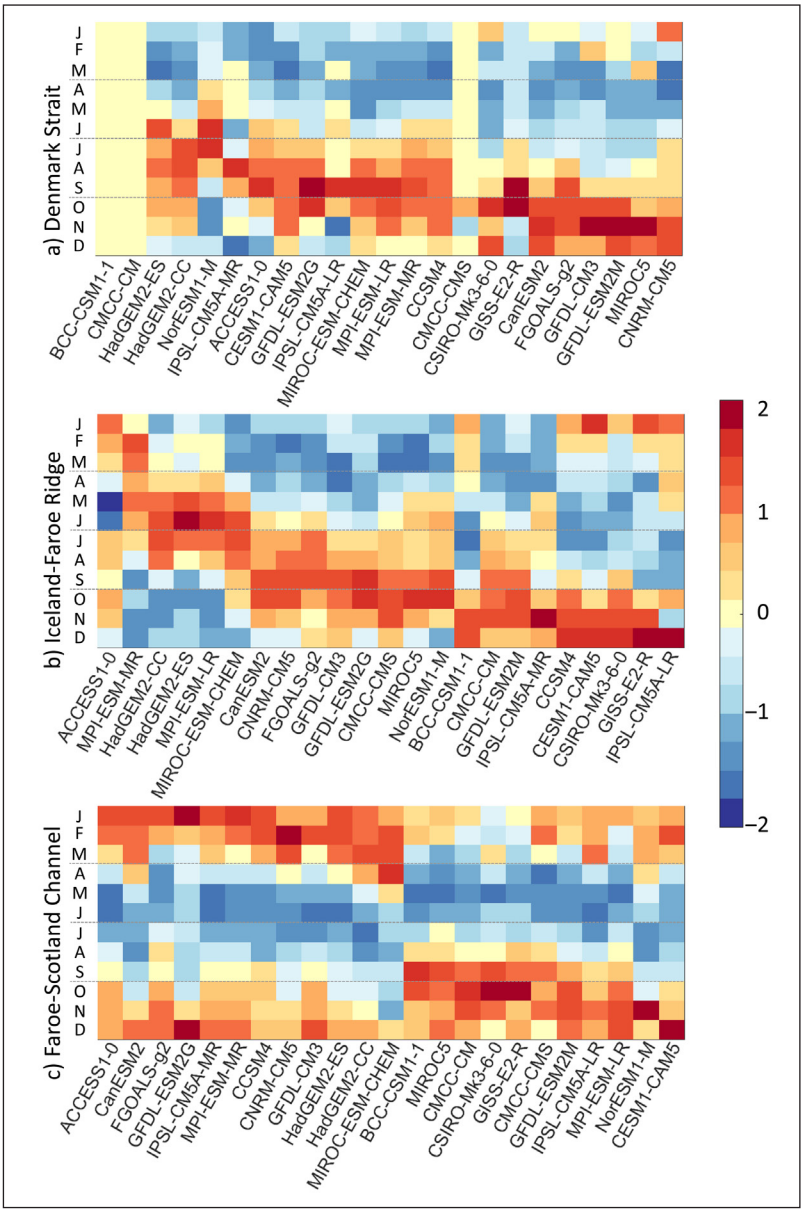

Figure 3: Across-model differences in seasonal cycle of heat transport through the gateways. For the 23 CMIP5 models, normalised seasonal cycle of the heat inflow across the three straits, ordered by month of the maximum inflow (red colours). Consequently, the model order on the x-axis differs for each strait and differs from that of Figure 2. DOI: https://doi.org/10.1525/elementa.354.f3

North Atlantic ocean dynamics, and the modelled North Atlantic atmospheric variability. We find that the inter-model differences in poleward heat transport across the GSR can be somewhat predicted by sorting all the CMIP5 models according to these three factors, starting by their effective resolution.

The impact of resolution

The Greenland-Scotland ridge consists of three narrow straits that are between 300 and 450 km wide. Intuitively, we therefore expect a relationship between the effective resolution of a model and its representation of the ridge, including the heat transport across it: the lowest resolution models should have the largest biases. The relationship between effective resolution (given in **Table 1**) and the mean heat transport (**Figure 2**) is not perfect, but is most obvious in Denmark Strait, which is the GSR strait the most inconsistently represented by the CMIP5 models, with a coast-to-coast distance ranging from just under 200 km for GISS-E2-R to more than 600 km for MIROC-ESM-CHEM (**Figure 4**). The models with weak transports do have low resolution (IPSL-LR and -MR, CMCC-CM and -CMS) and/or a too narrow strait (e.g. GISS-E2-R, **Figure 4**). Conversely, models with strong transports have higher resolution. Note that we do not find that the higher the resolution, the more accurate the modelled heat transport. Rather we find biases of opposite signs depending on the resolution, which is in agreement and can be explained

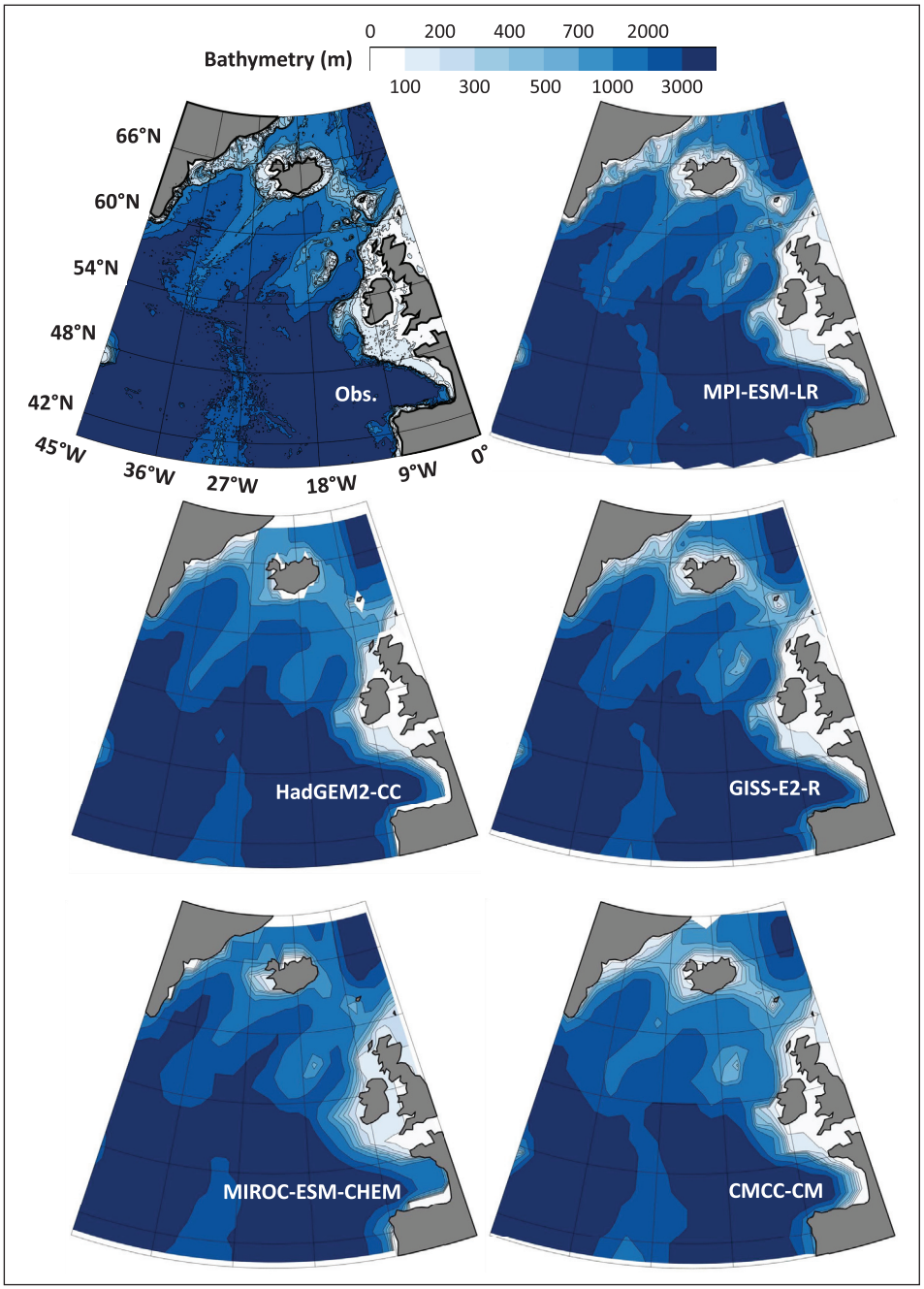

Figure 4: North Atlantic bathymetry from observations and in five representative CMIP5 models. Bathymetry from www.gebco.net. The five models were selected as having characteristic biases, as discussed in the text (see "The impact of resolution"). DOI: https://doi.org/10.1525/elementa.354.f4

by the finding of Menary et al. (2015) that the modelled North Atlantic is too warm in high resolution CMIP5 models and too cold in low resolution models.

In FSC, models with low resolution also have inflows that are too weak. Those with a resolution higher than 1° have a better representation of the bathymetric features south of the Faroe Islands (the Wyville Thomson Ridge; see e.g. MPI-ESM-LR in **Figure 4**). The models with the weakest transports are again the four with the coarsest resolution (IPSL-LR and -MR, and CMCC-CM and -CMS), in addition to GISS-E2-R which has the Faroe Islands further south than they ought to be. At the other end of the spectrum, FGOALS-g2 and MIROC-ESM-CHEM probably have stronger heat transports than other models with similar resolution because they have no Faroe Islands to restrict the inflow.

In IFR, however, no relationship can be seen between the mean heat transport and the effective resolution, probably because this strait is relatively well represented in the models (**Figure 4**). Half of the models have a strait width within 20 km of that observed. Even the models with the Faroe Islands underwater or at the wrong location have an acceptable heat transport across the IFR.

The bathymetry controls the width of the section, and hence constrains the heat transported through the individual sections. The orientation and depth of the sections, and in particular the presence or absence of bathymetric features, determine which water mass with which hydrographic properties can go through each section. But the representation of bathymetry outside of the GSR, notably the mid-Atlantic Ridge, is also crucial as it impacts the large scale-ocean circulation and ultimately determines which water mass will feed the various straits of the GSR (Hansen and Østerhus, 2000). This aspect is what we investigate next.

Dynamics of GSR heat transport

Source regions

As observed (Hansen and Østerhus, 2000), different source regions feed the three straits of the GSR. Because the routing from these sources to the GSR is highly bathymetry-dependent, and that the bathymetry in the models is not properly represented (see the mid-Atlantic Ridge on **Figure 4**), we expect the routing to be inaccurate in some models. In order to test this hypothesis, we backtracked the waters that we find at the GSR to their upstream origin. **Figure 5** shows over the North Atlantic

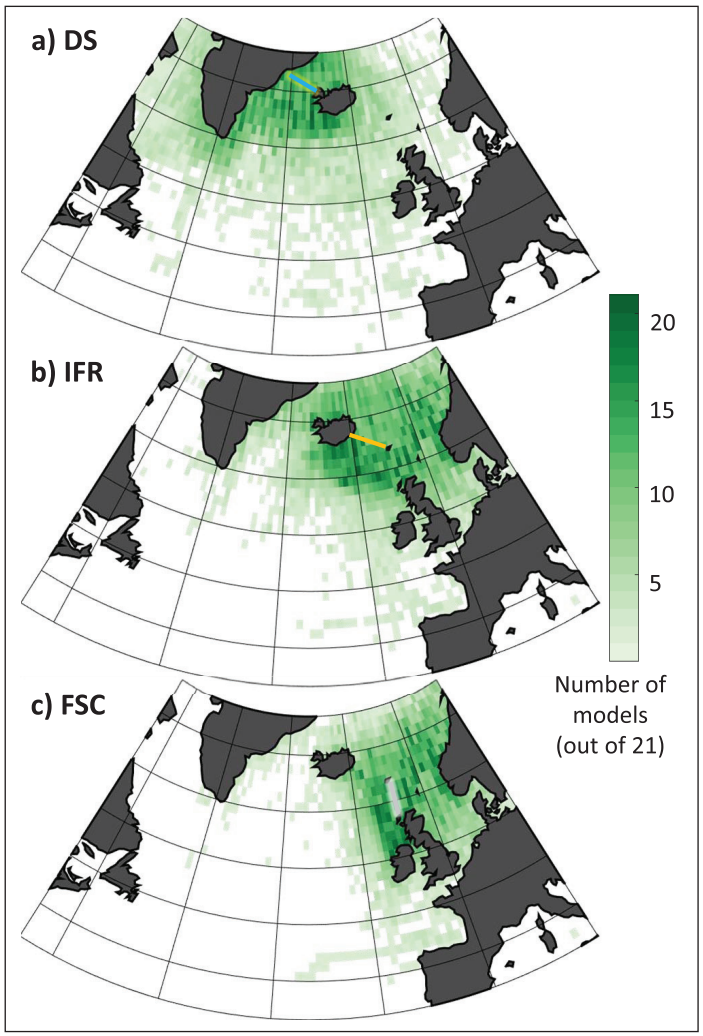

Figure 5: Source region of the water that flows through the Greenland-Scotland ridge in climate models. For each grid cell, number of models for which the water from that cell eventually flows through Denmark Strait (DS, top), the Iceland-Faroe ridge (IFR, middle) or the Faroe-Scotland channel (FSC, bottom) during 1986–2005 (see Methods and Figure S1). DOI: https://doi.org/10.1525/elementa.354.f5

how many models import water from a given grid cell (the more intense the green, the more models), while Figure S1 shows the details of the individual models.

There is a large spread for DS, with the majority of models importing water from the Irminger or Labrador seas, but also the European slope for seven models (**Figure 5**). These models are, in fact, those with the largest heat transport (supp. Figure S1), which is not surprising as water originating from the European slope is warmer than that from the other regions (Hátún et al., 2005). The same split is found for IFR, whereas FSC has only one model where the source water comes from west of Iceland; for the others, it comes from the European slope.

What does this mean? Different sources yield distinct temperatures Θ of the water flowing through the straits, resulting in heat transport changes ($\overline{V}\Theta'$, where V denotes the velocity; overbar, the mean value; and prime, the anomaly). However, heat transport anomalies can also occur as a result of changes in volume transport ($V'\overline{\Theta}$), or through eddy fluxes ($V'\Theta'$). In monthly CMIP5 model output, where eddy fluxes cannot be estimated with certainty, we find that the main driver for heat transport anomalies on both the seasonal and interannual time scales is changes in volume transport, with a time series correlation (not shown) exceeding 0.9 in all three straits for all models. That is, the stronger (faster) the volume transport, the stronger the heat transport. The majority of models also have a positive correlation between heat transport and temperature, although the correlation is less strong than that with volume transport (average of 0.5, not shown). These findings are in agreement with observations from the Nordic Seas (Skagseth et al., 2008; Årthun et al., 2012), and suggest that the biases in heat transport are not dominated by the different source waters, but rather by different velocities. We investigate this point further in the next section.

Large-scale oceanic and atmospheric drivers

As heat transport and volume transport are intimately linked, we now investigate whether the drivers of modelled heat transport and potential causes for its biases are associated with two metrics of large-scale ocean circulation: the strength of the subpolar gyre and the Atlantic Meridional Overturning Circulation. Several previous modelling studies have suggested that variations in the SPG and AMOC are reflected in oceanic heat transport changes through the Nordic Seas and into the Arctic (e.g. Hátún et al., 2005; Koenigk and Brodeau 2014). The sign of the correlation depends on the strait considered: DS receives a larger inflow when the subpolar gyre is strong (Hansen and Østerhus, 2000), whereas FSC receives a larger inflow when the subpolar gyre is weak (Hátún et al., 2005).

Consequently, in DS and FSC, the models can be split into the following two categories (**Figure 6**):

- Models with a negative correlation between the heat transport into the Nordic Seas and the Subpolar Gyre Index have a stronger heat transport than other models with the same effective resolution. The warm waters from the European slope current that feeds the GSR in these models (Figure S1) penetrate further north when the subpolar gyre is weak;
- In contrast, models with a positive correlation between the heat transport into the Nordic Seas and the Subpolar Gyre Index have a weaker heat transport than expected from their resolution, as these models tend to be fed by the subpolar North Atlantic (**Figures 5** and S1).

The AMOC also plays a role: strong heat transport is associated with a strong AMOC, especially in FSC (**Figure 6c**); weak heat transport, with a weak AMOC. The relationship between SPG/AMOC and heat transport is weaker for IFR (**Figure 6b**). However, even though the interannual variability of the heat transport and the AMOC/SPG are significantly correlated (colour of the dots on **Figure 6**), the mean values are not.

To further assess the spread in the mean values, we look at the dominant modes of atmospheric variability: the North Atlantic Oscillation, East-Atlantic pattern and Scandinavian pattern. There have been many studies linking the NAO to the GSR inflows (e.g. Zhang et al., 2004; Hansen et al., 2008; Langehaug et al., 2012). In agreement with that of Hansen et al. (2008), most CMIP5 models exhibit a negative correlation between the heat transport in DS and the NAO, and a positive correlation in FSC (**Figure 7**, left). That is, a stronger low-pressure anomaly south of Iceland associated with a positive NAO drives increased heat transport through the FSC and decreased through the DS. In both DS and IFR, the models with the strongest mean heat transports are, on average, in a negative phase of the NAO. Admittedly, all but four models are in a negative phase of the NAO over our study period, so this result may not be robust. The average EA pattern is also in a negative phase for all but four models (different from those of the NAO, **Figure 7** middle). Most models exhibit a positive correlation between the heat transport and the EA time series in DS, and negative in IFR and FSC. That is, a stronger low-pressure anomaly in the subpolar North Atlantic associated with a positive EA drives less inflow though the IFR and FSC. Although not studied in detail here, the relationship between the EA and heat transport across the GSR could be a result of EA-driven changes in the strength and size of the SPG (Langehaug et al., 2012; Barrier et al., 2014), which regulates heat transport into the Nordic Seas (**Figure 6** and Hátún et al., 2005). Finally, SCA is the mode with the least across-model consistency (**Figure 7** right), with eight models in a positive phase and no agreement in the sign of the correlation between the heat transport and SCA time series. There is no agreement in the literature either about the influence of SCA on ocean circulation. In a fully coupled model, Medhaug et al. (2012) found that SCA results in stronger poleward heat transport across the GSR, whereas Barrier et al. (2014) found no significant ocean response in a forced model.

In addition to the magnitude or phase of the atmospheric driver, the spatial pattern may also influence the heat transport. Davini and Cagnazzo (2014) and Ning and Bradley (2016) found that there are "slight" differences in the location of the centre of action in the spatial patterns of the atmospheric modes. Looking at the composite

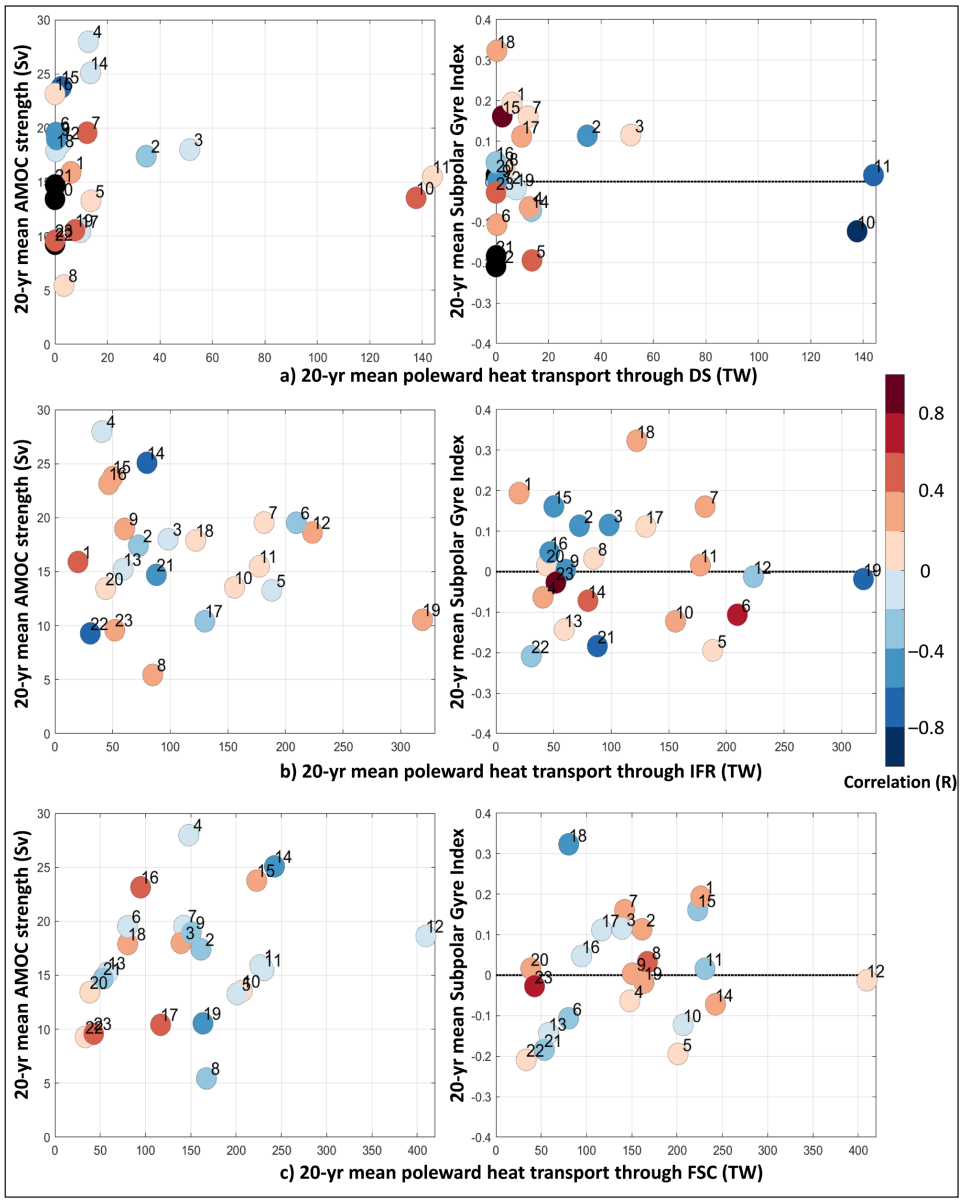

Figure 6: Oceanic drivers of modelled inaccuracies in poleward heat transport through the Greenland-Scotland ridge. For each CMIP5 model identified by their number as in Table 1, relationship between the 20 year mean poleward heat transport and the 20 year mean oceanic driver value (left: Atlantic Meridional Overturning Circulation, AMOC; right: Subpolar Gyre), colour coded by the correlation of their 12-month low-pass filtered time series in **a)** Denmark Strait (DS); **b)** Iceland-Faroe ridge (IFR); and **c)** Faroe-Scotland Channel (FSC). DOI: https://doi.org/10.1525/elementa.354.f6

map of the five models with the strongest heat transports versus the weakest heat transports (**Figure 8**), these differences seem to matter. For NAO, the difference is most pronounced when looking at the DS inflow (**Figure 8a**); the low-pressure center is shifted south-east, towards the central Atlantic, for weak transports. For EA, the differences in inflow strength are more related to a strengthening of the low-pressure center just west of Ireland; there is also a slight south-west shift from a centre just West of Ireland for the strongest inflows to the central Atlantic for the weakest ones (**Figure 8b**). For SCA, the weakest transports have their centre of action shifted southwest towards the central Atlantic, away from their "normal" position over Scandinavia (**Figure 8c**). To the best of our knowledge, only the latter relationship between the location of SCA and the strength of the GSR inflow has been studied in fully coupled climate models (Medhaug et al., 2012), but the results are nevertheless not surprising. As explained by Hansen et al. (2008), the GSR inflow can only be moved by two forces: the surface stress generated by the wind; and the pressure gradient, generated by a sloping sea surface, i.e. also indirectly by the wind. Hence, the relative location of the low and high pressure systems that define the atmospheric patterns can influence the heat transport into the Nordic Seas by controlling the wind stress over the GSR. Moreover, the wind stress also influences the subpolar gyre circulation (e.g. Langehaug et al., 2012) and the GSR overflows (e.g. Zhang et al., 2004), which indirectly drive inflow changes across the GSR (Hansen et al., 2008; Langehaug et al., 2012).

In summary, the relative strength of the poleward oceanic heat transport across the GSR in CMIP5 models can be roughly predicted by sorting the models first by their effective resolution and their representation of the

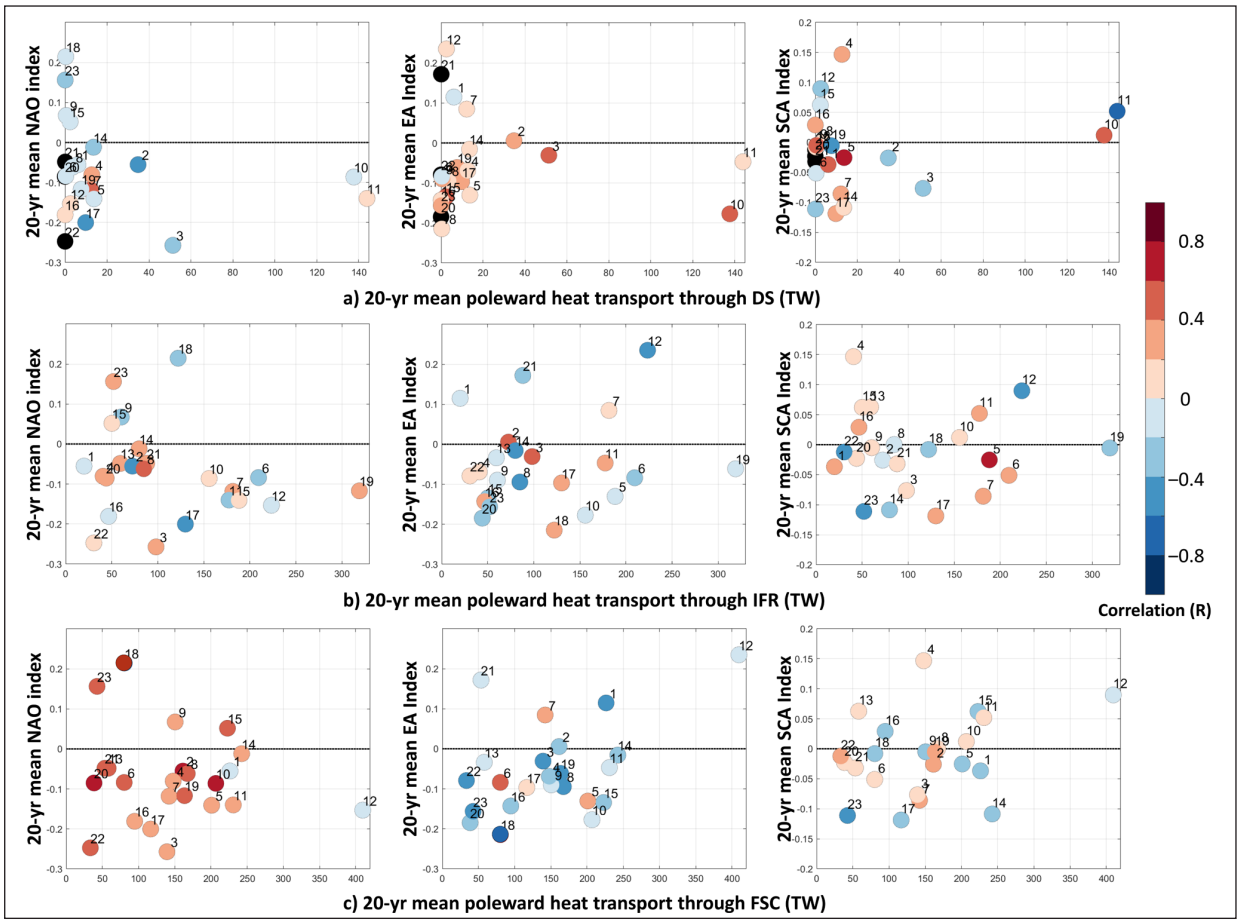

Figure 7: Atmospheric drivers of modelled inaccuracies in heat transport through the Greenland-Scotland ridge. For each CMIP5 model identified by their number as in Table 1, relationship between the 20 year mean poleward heat transport and the 20 year mean atmospheric driver value (left: North Atlantic Oscillation, NAO; centre: East Atlantic pattern, EA; right: Scandinavian pattern, SCA), colour coded by the correlation of their 12-month low-pass filtered time series in a) Denmark Strait (DS); b) Iceland-Faroe ridge (IFR); and c) Faroe-Scotland Channel (FSC). DOI: https://doi.org/10.1525/elementa.354.f7

bathymetry, which to a large extent controls which source region feeds the GSR. Mismatch between the resolution and the heat transport are related to sign of their correlation with the oceanic indices and the location of their atmospheric centres of action.

Discussion: suggestions to improve the models

Our findings show that the poleward oceanic heat transport from the subpolar North Atlantic to the Nordic Seas is not represented correctly in CMIP5 models. In agreement with Menary et al. (2015) we find that increasing the resolution is important, but not sufficient. The key for reducing biases instead appears to be to import water from the correct source. As pointed out by Langehaug et al. (2012), importing water from the correct source in models is not a simple task as it depends not only on the correct representation of the mid-Atlantic Ridge (Hansen and Østerhus, 2000), but also on that of the surface heat and freshwater fluxes, which depend notably on where models melt sea ice. Interestingly, the models that import water from the wrong source in our study are also the ones that have deep convection at the wrong location in the North Atlantic (Heuzé 2017), which was explained by their inaccurate representation of sea ice. A strong relationship exists between ocean heat transport across the GSR and subsequent sea ice cover (e.g. Årthun et al., 2012; Yeager et al., 2015); whether, the GSR heat transport needs to be improved to improve the sea ice representation, or whether a better modelled sea ice cover would improve the modelled large-scale ocean circulation and, hence, the GSR heat transport is therefore not clear.

Improving the representation of the bathymetry is not that straightforward either. Rather than pushing for an increase in resolution, we believe that different approaches to improve model bathymetry, such as the use of porous grids or overflow parameterisations (Snow et al., 2015), could lead to improved model output. More diversity among model vertical grid types is also encouraged: terrain-following models may perform better than those with a fixed-depth grid, but the latter form the vast majority of the CMIP5 models (**Table 1**). We also strongly recommend that passive tracer output become routinely archived and distributed in CMIP6, in order to facilitate future transport studies; Lagrangian backtracking using monthly mean fields without considering eddies or diffusion as we did here is the best that can be done with CMIP5 data, but is not ideal.

Even harder but maybe most important is to improve the representation of the atmosphere. We found in particular that models with strong or weak inflows had

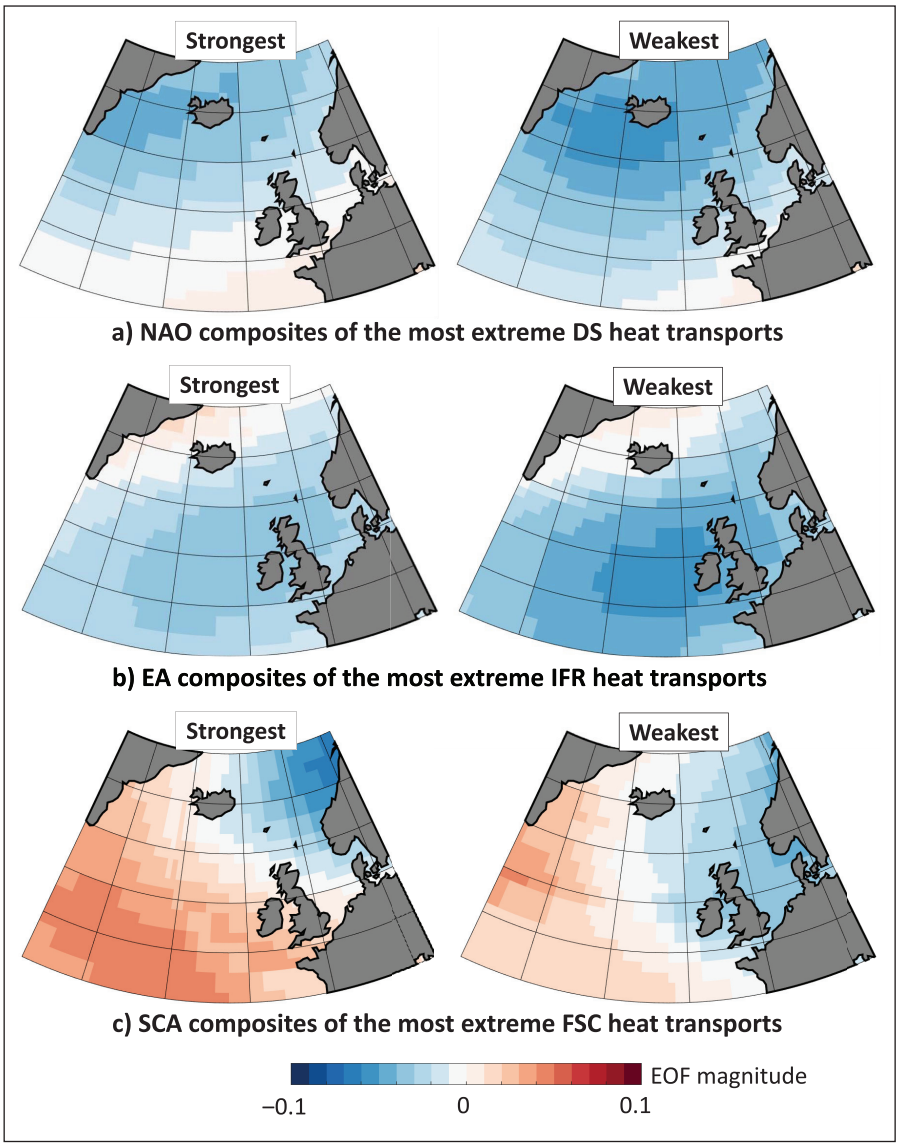

Figure 8: Geographical differences in atmospheric drivers between strong and weak heat transports. For each strait: **a)** Denmark Strait (DS), **b)** Iceland-Faroe ridge (IFR), and **c)** Faroe-Scotland channel (FSC), composite maps of the atmospheric mode of variability where the five models with the strongest (left) and weakest (right) heat transport showed the largest difference. DOI: https://doi.org/10.1525/elementa.354.f8

different centres of action for their NAO, EA and SCA, i.e. for the wind stress curl. Forced high-resolution ocean models simulate well the Atlantic inflow to the Nordic Seas (e.g., Sandø et al., 2012), suggesting that a realistic atmospheric circulation variability is key to successfully simulate the inflow. The review by Furevik and Nilsen (2005) lists some processes that contribute to atmospheric variability:

1) non-linear processes in the troposphere (eddies), which highlights again the need for higher resolution and/or more ensemble members for each model;
2) the stratosphere, which in general is not included in CMIP5 models (Heuzé, 2017);
3) sea surface temperature and/or sea ice cover, which in fact are also partly controlled by the atmosphere (e.g. Langehaug et al., 2012);
4) and global midlatitude–tropics teleconnections.

The many feedbacks involved, from the stratosphere to the deep ocean (Haase et al., 2018), means that identifying the single most important bias is nearly impossible. Soon, however, results from the CMIP6 experiments will be released (Eyring et al., 2016), and the many dedicated forced MIPs should at least allow for the identification of the model component that is most crucial to get right.

Finally, as models are tuned and evaluated with respect to observational datasets, we have to bear in mind that these are few and limited in time. The datasets used in this study contain fewer than 25 years of continuous observations, which is too short to capture any long term variability. Furthermore, the majority of sub-surface velocity observations are based on mooring measurements with limited horizontal and vertical resolution. Maintaining these continuous time series are maintained, and further complementing them with higher resolution observations from,

for example, sea gliders (Høydalsvik et al., 2013; Lozier et al., 2017), is therefore crucial for present and future climate studies.

Summary and conclusions

The representation of the poleward ocean heat transport from the North Atlantic into the Nordic Seas across the Greenland-Scotland ridge has a large spread in mean value, interannual variability, and both magnitude and phase of the seasonal cycle. The reason for this spread depends on the strait of the GSR considered. In Denmark Strait, the resolution is key, with high resolution being associated with strong transport, and low resolution and/or a too narrow strait with weak heat transport. In the Faroe-Scotland channel the linear relationship between resolution and heat transport is only valid for models coarser than 1°. The resolution has no significant impact on the Iceland Faroe ridge, where the relative strength of the modelled heat transport can be predicted from determining the source of the water flowing through the IFR. We find that the strongest heat transports are associated with water predominantly originating from the European slope current, whereas models with weak heat transport are more influenced by the subpolar gyre region. The source region is also key for DS, with the strongest heat transports associated with a source south of Iceland, and the weakest from the Labrador region. In agreement with observations (Hansen and Østerhus, 2000), FSC is mainly fed from the European slope current. For all three straits, ocean dynamics, source region, and heat transport are tightly connected: models importing water from the Labrador region have stronger heat transport when the subpolar gyre is strong, whereas those importing water from the European slope current, i.e. more from the subtropical gyre, benefit from a weak gyre. Moreover, the atmospheric dynamics, and in particular the relative location of the low/high pressure systems, are also crucial. Models with too-weak heat transports have their low pressure system shifted towards the central Atlantic, thus shifting the wind stress that controls the inflow (Biastoch et al., 2003; Richter et al., 2012; Sandø et al., 2012), but also affecting the SPG and the overall water mass characteristics in the North Atlantic (Furevik and Nilsen, 2005; Langehaug et al., 2012).

Multi-model assessments, as presented here, and the identification of across-model similarities and differences, are important in order to improve climate models. The large spread in modelled poleward ocean heat transport highlights the uncertainty in future projections of ocean heat transport and associated climate impacts (Burgard and Notz, 2017; Onarheim and Årthun, 2017; Yeager and Robson, 2017; Oldenburg et al., 2018), and needs to be simulated more accurately in the next generation of climate models. Based on our results, the modelled ocean heat transport will likely benefit from improved bathymetry, although increasing the resolution can also induce other biases (e.g. this study and (Menary et al., 2015), and from improved atmosphere-ice-ocean interaction, potentially through a more systematic inclusion of the stratosphere in the atmosphere component (e.g. Haase et al., 2018).

Data Accessibility Statement

All CMIP5 outputs can be freely downloaded from any Earth System Grid Federation partner website; those used in this study were retrieved from that of DKRZ (https://cera-www.dkrz.de/). The SODA reanalysis data sets are available through www.soda.umd.edu, whereas GECCO2 and OraS4 are available through the CliSAP-Integrated Climate Data Center (http://icdc.cen.uni-hamburg.de/). The scripts for computing the heat transport and tracking the source of the inflows are available on C.H. personal website: http://cheuze.com/scripts-data.

Supplemental file

The supplemental file for this article can be found as follows:

- **Figure S1.** Source region of the water that flows though the Greenland-Scotland ridge in each CMIP5 model. DOI: https://doi.org/10.1525/elementa.354.s1

Acknowledgements

We acknowledge the World Climate Research Programme's Working Group on Coupled Modelling, which is responsible for CMIP, and we thank the climate modelling groups (whose models are listed in Table 1 of this paper) for producing and making available their model output. We thank the two anonymous reviewers whose suggestions significantly increased the readability of this study. The authors thank L.H. Smedsrud for the constructive discussion at EGU2017 that strongly inspired this paper.

Funding information

C.H. is funded by a VINNOVA Marie Curie Cofund fellowship (Dnr. 2015-01487) and the Research Council of Sweden project WAOW (Dnr. 2018-03859). M.Å is funded by the Research Council of Norway project PATHWAY (grant 263223), and the Blue-Action project (European Union's Horizon 2020 research and innovation program, grant number: 727852).

Competing interests

The authors have no competing interests, as defined by Elementa, that might be perceived to influence the research presented in this manuscript.

Author contributions

- Contributed to conception and design: CH, MÅ
- Contributed to acquisition of data: CH for CMIP5, MÅ for ocean reanalyses
- Contributed to analysis and interpretation of data: CH, MÅ
- Drafted and/or revised the article: CH, MÅ
- Approved the submitted version for publication: CH

References

Årthun, M, Eldevik, T, Smedsrud, LH, Skagseth, Ø and **Ingvaldsen, RB.** 2012. Quantifying the influence of Atlantic heat on Barents Sea ice variability and

retreat. *J Climate* **25**: 4736–4743. DOI: https://doi.org/10.1175/JCLI-D-11-00466.1

Årthun, M, Eldevik, T, Viste, E, Drange, H, Furevik, T, Johnson, HL and **Keenlyside, NS.** 2017. Skillful prediction of northern climate provided by the ocean. *Nat Commun* **8**: 875. DOI: https://doi.org/10.1038/ncomms15875

Balmaseda, MA, Mogensen, K and **Weaver, AT.** 2013. Evaluation of the ECMWF ocean reanalysis system Oras4. *Q J R Meteorol Soc* **136**: 1132–1161. DOI: https://doi.org/10.1002/qj.2063

Barnston, A and **Livezey, R.** 1987. Classification, seasonality and persistence of low frequency atmospheric circulation patterns. *MonthlyWeather Rev* **115**: 1083–1126. DOI: https://doi.org/10.1175/1520-0493(1987)115<1083:CSAPOL>2.0.CO;2

Barrier, N, Cassou, C, Deshayes, J and **Treguier, A.** 2014. Response of North Atlantic Ocean circulation to atmospheric weather regimes. *J Phys Ocean* **44**: 179–201. DOI: https://doi.org/10.1175/JPO-D-12-0217.1

Berx, B, Hansen, B, Østerhus, S, Larsen, KM, Sherwin, T and **Jochumsen, K.** 2013. Combining in situ measurements and altimetry to estimate volume, heat and salt transport variability through the Faroe-Shetland Channel. *Ocean Science* **9**(4): 639. DOI: https://doi.org/10.5194/os-9-639-2013

Biastoch, A, Käse, RH and **Stammer, DB.** 2003. The sensitivity of the Greenland Scotland Ridge overflow to forcing changes. *J Phys Oceanogr* **33**: 2307–2319. DOI: https://doi.org/10.1175/1520-0485(2003)033<2307:TSOTGR>2.0.CO;2

Brambilla, E and **Talley, L.** 2006. Surface drifter exchange between the North Atlantic subtropical and subpolar gyres. *J Geophys Res Oceans* **11**: C07026. DOI: https://doi.org/10.1029/2005JC003146

Burgard, C and **Notz, D.** 2017. Drivers of Arctic Ocean warming in CMIP5 models. *Geophys Res Lett* **44**: 4263–4271. DOI: https://doi.org/10.1002/2016GL072342

Carton, JA and **Giese, BS.** 2008. A reanalysis of ocean climate using Simple Ocean Data Assimilation (SODA). *Mon Wea Rev* **136**: 2999–3017. DOI: https://doi.org/10.1175/2007MWR1978.1

Collins, M, Botzet, M, Carril, A, Drange, H, Jouzeau, A, Latif, M, Masina, S, Otteraa, O, Pohlmann, H and **Sorteberg, A.** 2006. Interannual to decadal climate predictability in the North Atlantic: a multimodel-ensemble study. *J Climate* **19**: 1195–1203. DOI: https://doi.org/10.1175/JCLI3654.1

Danabasoglu, G, Large, W and **Briegleb, B.** 2010. Climate impacts of parameterized Nordic Sea overflows. *J Geophys Res Oceans* **115**: C1. DOI: https://doi.org/10.1029/2010JC006243

Davini, P and **Cagnazzo, C.** 2014. On the misinterpretation of the North Atlantic Oscillation in CMIP5 models. *Climate Dyn* **43**(5–6): 1497–1511. DOI: https://doi.org/10.1007/s00382-013-1970-y

Deshayes, J, Curry, R and **Msadek, R.** 2014. CMIP5 model intercomparison of fresh water budget and circulation in the North Atlantic. *J Climate* **27**: 3298–3317. DOI: https://doi.org/10.1175/JCLI-D-12-00700.1

Dickson, RR and **Brown, J.** 1994. The production of North Atlantic Deep Water: sources, rates, and pathways. *J Geophys Res* **99**: 12319–12341. DOI: https://doi.org/10.1029/94JC00530

Drijfhout, S, Vries, PD, Döös, K and **Coward, A.** 2003. Impact of eddy-induced transport on the Lagrangian structure of the upper branch of the thermohaline circulation. *J Phys Ocean* **33**: 2141–2155. DOI: https://doi.org/10.1175/1520-0485(2003)033<2141:IOETOT>2.0.CO;2

Eldevik, T, Nilsen, JEØ, Iovino, D, Olsson, KA, Sandø, AB and **Drange, H.** 2009. Observed sources and variability of Nordic seas overflow. *Nat Geosci* **2**: 405–409. DOI: https://doi.org/10.1038/ngeo518

Eyring, V, Bony, S, Meehl, GA, Senior, CA, Stevens, B, Stouffer, RJ and **Taylor, KE.** 2016. Overview of the Coupled Model Intercomparison Project Phase 6 (CMIP6) experimental design and organization. *Geoscientific Model Development* **9**: 1937–1958. DOI: https://doi.org/10.5194/gmd-9-1937-2016

Flato, G, Marotzke, J, Abiodun, B, Braconnot, P and **Chou, SC.** 2013. Chap. Evaluation of Climate Models. In: *Climate Change 2013: The Physical Science Basis. Contribution of Working Group I to the Fifth Assessment Report of the Intergovernmental Panel on Climate Change*. Cambridge University Press, Cambridge, United Kingdom and New York, NY, USA.

Fofonoff, NP and **Millard, R, Jr.** 1983. Algorithms for the computation of fundamental properties of seawater. Paris: UNESCO.

Furevik, T and **Nilsen, J.** 2005. Chap. Large-scale atmospheric circulation variability and its impacts on the Nordic Seas Ocean climate – A review. In: *Geophysical Monograph*. Vol 158. American Geophysical Union. DOI: https://doi.org/10.1029/158GM09

Guo, C, Ilicak, M, Bentsen, M and **Fer, I.** 2016. Characteristics of the Nordic Seas overflows in a set of Norwegian Earth System Model experiments. *Ocean Mod* **104**: 112–128. DOI: https://doi.org/10.1016/j.ocemod.2016.06.004

Haase, S, Matthes, K, Latif, M and **Omrani, N.** 2018. The importance of a properly represented stratosphere for northern hemisphere surface variability in the atmosphere and the ocean. *J Climate* **31**: 8481–8497. DOI: https://doi.org/10.1175/JCLI-D-17-0520.1

Häkkinen, S and **Rhines, P.** 2004. Decline of subpolar North Atlantic circulation during the 1990s. *Science* **304**: 555–559. DOI: https://doi.org/10.1126/science.1094917

Hansen, B, Hátún, H, Kristiansen, R, Olsen, S and **Østerhus, S.** 2010. Stability and forcing of the Iceland-Faroe inflow of water, heat, and salt to the Arctic. *Ocean Sci* **6**: 1013–1026. DOI: https://doi.org/10.5194/os-6-1013-2010

Hansen, B, Larsen, KMH, Hátún, H, Kristiansen, R, Mortensen, E and **Østerhus, S.** 2015. Transport of volume, heat, and salt towards the Arctic in the Faroe Current 1993–2013. *Ocean Sci* **11**: 743. DOI: https://doi.org/10.5194/os-11-743-2015

Hansen, B and **Østerhus, S.** 2000. North Atlantic–Nordic seas exchanges. *Progr Oceanogr* **45**: 109–208. DOI: https://doi.org/10.1016/S0079-6611(99)00052-X

Hansen, B, Østerhus, S, Hátún, H, Kristiansen, R and **Larsen, K.** 2003. The Iceland-Faroe inflow of Atlantic water to the Nordic seas. *Progr Oceanogr* **59**: 443–474. DOI: https://doi.org/10.1016/j.pocean.2003.10.003

Hansen, B, Østerhus, S, Turrell, WR, Jónsson, S, Valdimarsson, H, Hátún, H and **Olsen, SM.** 2008. Chap. The inflow of Atlantic water, heat, and salt to the nordic seas across the Greenland–Scotland ridge. In: *Arctic–Subarctic Ocean Fluxes*, 15–43. Netherlands: Springer. DOI: https://doi.org/10.1007/978-1-4020-6774-7_2

Hátún, H and **Chafik, L.** 2018. On the recent ambiguity of the North Atlantic subpolar gyre index. *J Geophys Res* **123**. DOI: https://doi.org/10.1029/2018JC014101

Hátún, H, Sandø, AB, Drange, H, Hansen, B and **Valdimarsson, H.** 2005. Influence of the Atlantic subpolar gyre on the thermohaline circulation. *Science* **309**: 1841–1844. DOI: https://doi.org/10.1126/science.1114777

Heuzé, C. 2017. North Atlantic deep water formation and AMOC in CMIP5 models. *Ocean Sci* **13**: 609–622. DOI: https://doi.org/10.5194/os-13-609-2017

Høydalsvik, F, Mauritzen, C, Orvik, KA, LaCasce, JH, Lee, CM and **Gobat, J.** 2013. Transport estimates of the Western Branch of the Norwegian Atlantic Current from glider surveys. *Deep Sea Res* **79**: 86–95. DOI: https://doi.org/10.1016/j.dsr.2013.05.005

Hurrell, J. 1995. Decadal trends in the North Atlantic Oscillation: regional temperatures and precipitation. *Science* **269**: 676–679. DOI: https://doi.org/10.1126/science.269.5224.676

Jónsson, S and **Valdimarsson, H.** 2012. Water mass transport variability to the North Icelandic shelf, 1994–2010. *ICES Journal of Marine Science* **69**(5): 809–815. DOI: https://doi.org/10.1093/icesjms/fss024

Koenigk, T and **Brodeau, L.** 2014. Ocean heat transport into the Arctic in the twentieth and twenty-first century in EC-Earth. *Climate Dynamics* **42**(11–12): 3101–3120. DOI: https://doi.org/10.1007/s00382-013-1821-x

Köhl, A. 2015. Evaluation of the GECCO2 ocean synthesis: transports of volume, heat and freshwater in the Atlantic. *Quarterly Journal of the Royal Meteorological Society* **141**(686): 166–181. DOI: https://doi.org/10.1002/qj.2347

Langehaug, H, Matei, D, Eldevik, T, Lohmann, K and **Gao, Y.** 2017. On model differences and skill in predicting sea surface temperature in the Nordic and Barents Seas. *Clim Dyn* **48**: 913–933. DOI: https://doi.org/10.1007/s00382-016-3118-3

Langehaug, H, Medhaug, I, Eldevik, T and **Otterå, O.** 2012. Arctic/Atlantic exchanges via the subpolar gyre. *J Climate* **25**: 2421–2439. DOI: https://doi.org/10.1175/JCLI-D-11-00085.1

Langehaug, H, Rhines, P, Eldevik, T, Mignot, J and **Lohmann, K.** 2012. Water mass transformation and the North Atlantic Current in three multicentury climate model simulations. *J Geophys Res Oceans* **117**: C11001. DOI: https://doi.org/10.1029/2012JC008021

Li, D, Zhang, R and **Knutson, TR.** 2017. On the discrepancy between observed and CMIP5 multi-model simulated Barents Sea winter sea ice decline. *Nat Comm* **8**: 14991. DOI: https://doi.org/10.1038/ncomms14991

Lozier, S, Bacon, S, Bower, AS, Cunningham, SA, De Jong, F, De Steur, L, Deyoung, B, Fischer, J, Gary, S, Greenan, B, Heimbach, P, Holliday, NP, Houpert, L, Inall, ME, Johns, WE, Johnson, HL, Karstensen, J, Li, F, Lin, X, Mackay, N, Marshall, DP, Mercier, H, Myers, PG, Pickart, RS, Pillar, HR, Straneo, F, Thierry, V, Weller, RA, Williams, RG, Wilson, C, Yang, J, Zhao, J and **Zika, JD** 2017. Overturning in the Subpolar North Atlantic Program: a new international ocean observing system. *Bull Amer Met Soc* **98**(4): 737–752. DOI: https://doi.org/10.1175/BAMS-D-16-0057.1

Mahlstein, I and **Knutti, R.** 2011. Ocean heat transport as a cause for model uncertainty in projected Arctic warming. *J Geophys Res Oceans* **24**: 1451–1460. DOI: https://doi.org/10.1175/2010JCLI3713.1

Matei, D, Pohlmann, H, Jungclaus, J, Müller, W, Haak, H and **Marotzke, J.** 2012. Two tales of initializing decadal climate prediction experiments with the ECHAM5/MPIOM model. *J Climate* **25**: 8502–8523. DOI: https://doi.org/10.1175/JCLI-D-11-00633.1

Medhaug, I, Langehaug, H, Eldevik, T, Furevik, T and **Bentsen, M.** 2012. Mechanisms for decadal scale variability in a simulated Atlantic meridional overturning circulation. *Clim Dyn* **39**: 77–93. DOI: https://doi.org/10.1007/s00382-011-1124-z

Menary, MB, Hodson, DL, Robson, JI, Sutton, RT, Wood, RA and **Hunt, JA.** 2015. Exploring the impact of CMIP5 model biases on the simulation of North Atlantic decadal variability. *Geophys Res Lett* **42**: 5926–5934. DOI: https://doi.org/10.1002/2015GL064360

Menary, MB and **Wood, RA.** 2017. An anatomy of the projected North Atlantic warming hole in CMIP5 models. *Clim Dyn*, 1–18. DOI: https://doi.org/10.1007/s00382-017-3793-8

Ning, L and **Bradley, R.** 2016. NAO and PNA influences on winter temperature and precipitation over the eastern United States in CMIP5 GCMs. *Clim Dyn* **46**: 1257–1276. DOI: https://doi.org/10.1007/s00382-015-2643-9

Oldenburg, D, Armour, K, Thompson, LA and **Bitz, C.** 2018. Distinct mechanisms of ocean heat transport into the Arctic under internal variability and climate change. *Geophys Res Lett* **45**. DOI: https://doi.org/10.1029/2018GL078719

Olsen, SM, Hansen, B, Østerhus, S, Quadfasel, D and **Valdimarsson, H.** 2016. Biased thermohaline exchanges with the Arctic across the Iceland-Faroe Ridge in ocean climate models. *Ocean Sci* **12**: 545. DOI: https://doi.org/10.5194/os-12-545-2016

Onarheim, IH and **Årthun, M.** 2017. Toward an ice-free Barents Sea. *Geophys Res Lett* **44**(16): 8387–8395. DOI: https://doi.org/10.1002/2017GL074304

Onarheim, IH, Eldevik, T, Årthun, M, Ingvaldsen, RB and **Smedsrud, LH.** 2015. Skillful prediction of Barents Sea ice cover. *Geophys Res Lett* **42**: 5364–5371. DOI: https://doi.org/10.1002/2015GL064359

Orvik, KA and **Niiler, P.** 2002. Major pathways of Atlantic water in the northern North Atlantic and Nordic Seas toward Arctic. *Geophys Res Lett* **29**: 1–4. DOI: https://doi.org/10.1029/2002GL015002

Østerhus, S, Turrell, WR, Jónsson, S and **Hansen, B.** 2005. Measured volume, heat, and salt fluxes from the Atlantic to the Arctic Mediterranean. *Geophys Res Lett* **37**: L07603. DOI: https://doi.org/10.1029/2004GL022188

Richter, K, Segtnan, O and **Furevik, T.** 2012. Variability of the Atlantic inflow to the Nordic Seas and its causes inferred from observations of sea surface height. *J Geophys Res Oceans* **117**: C04004. DOI: https://doi.org/10.1029/2011JC007719

Sandø, AB, Gao, Y and **Langehaug, HR.** 2014. Poleward ocean heat transports, sea ice processes, and Arctic sea ice variability in NorESM1-M simulations. *J Geophys Res Oceans* **119**: 2095–2108. DOI: https://doi.org/10.1002/2013JC009435

Sandø, AB, Nilsen, J, Eldevik, T and **Bentsen, M.** 2012. Mechanisms for variable North Atlantic–Nordic seas exchanges. *J Geophys Res Oceans* **117**: C12006. DOI: https://doi.org/10.1029/2012JC008177

Schauer, U and **Beszczynska-Möller, A.** 2009. Problems with estimation and interpretation of oceanic heat transport–conceptual remarks for the case of Fram Strait in the Arctic Ocean. *Ocean Science* **5**: 487–494. DOI: https://doi.org/10.5194/os-5-487-2009

Skagseth, Ø, Furevik, T, Ingvaldsen, R, Loeng, H, Mork, KA, Orvik, KA and **Ozhigin, V.** 2008. Chap. Volume and heat transports to the Arctic Ocean via the Norwegian and Barents Seas. In: *Arctic–Subarctic Ocean Fluxes*. Netherlands: Springer. DOI: https://doi.org/10.1007/978-1-4020-6774-7_3

Snow, K, Hogg, AM, Downes, SM, Sloyan, BM, Bates, ML and **Griffies, SM.** 2015. Sensitivity of abyssal water masses to overflow parameterisations. *Ocean Modell* **89**: 84–103. DOI: https://doi.org/10.1016/j.ocemod.2015.03.004

Taylor, KE, Stouffer, RJ and **Meehl, GA.** 2012. An overview of CMIP5 and the experiment design. *Bull Amer Meteor Soc* **93**: 485–498. DOI: https://doi.org/10.1175/BAMS-D-11-00094.1

Uotila, P, Goosse, H, Haines, K, Chevallier, M, Barthélemy, A, Bricaud, C, Carton, J, Fučkar, N, Garric, G, Iovino, D, Kauker, F, Korhonen, M, Lien, VS, Marnela, M, Massonnet, F, Mignac, D, Peterson, KA, Sadikni, R, Shi, L, Tietsche, S, Toyoda, T, Xie, J and **Zhang, Z.** 2018. An assessment of ten ocean reanalyses in the polar regions. *Clim Dyn*, 1–38. DOI: https://doi.org/10.1007/s00382-018-4242-z

Yeager, SG, Karspeck, A and **Danabasoglu, G.** 2015. Predicted slow-down in the rate of Atlantic sea ice loss. *Geophys Res Lett* **42**: 10704–107137. DOI: https://doi.org/10.1002/2015GL065364

Yeager, SG and **Robson, JI.** 2017. Recent progress in understanding and predicting Atlantic decadal climate variability. *Curr Clim Change Rep* **3**: 112–127. DOI: https://doi.org/10.1007/s40641-017-0064-z

Zhang, J, Steele, M, Rothrock, D and **Lindsay, R.** 2004. Increasing exchanges at Greenland–Scotland Ridge and their links with the North Atlantic Oscillation and Arctic sea ice. *Geophys Res Lett* **31**: L09307. DOI: https://doi.org/10.1029/2003GL019304

How to cite this article: Heuzé, C and Årthun, M. 2019. The Atlantic inflow across the Greenland-Scotland ridge in global climate models (CMIP5). *Elem Sci Anth,* 7: 16. DOI: https://doi.org/10.1525/elementa.354

Domain Editor-in-Chief: Jody W. Deming, Department of Biological Oceanography, University of Washington, US

Associate Editor: Stephen F. Ackley, Department of Geological Sciences, University of Texas at San Antonio, US

Knowledge Domain: Ocean Science

Submitted: 21 August 2018 **Accepted:** 08 February 2019 **Published:** 21 May 2019

ELEMENTA Science of the Anthropocene

Elem Sci Anth is a peer-reviewed open access journal published by University of California Press.

OPEN ACCESS